



Heterogeneous & Homogeneous & Bio- & Nano-

CHEM **CAT** CHEM

CATALYSIS

Accepted Article

Title: Impact of the Oxygen Vacancies on Copper Electronic State and Activity of Cu-Based Catalysts in the Hydrogenation of Methyl Acetate to Ethanol

Authors: Yushan Xi, Yue Wang, Dawei Yao, Antai Li, Jingyu Zhang, Yujun Zhao, Jing Lv, and Xinbin Ma

This manuscript has been accepted after peer review and appears as an Accepted Article online prior to editing, proofing, and formal publication of the final Version of Record (VoR). This work is currently citable by using the Digital Object Identifier (DOI) given below. The VoR will be published online in Early View as soon as possible and may be different to this Accepted Article as a result of editing. Readers should obtain the VoR from the journal website shown below when it is published to ensure accuracy of information. The authors are responsible for the content of this Accepted Article.

To be cited as: *ChemCatChem* 10.1002/cctc.201900413

Link to VoR: <http://dx.doi.org/10.1002/cctc.201900413>

WILEY-VCH

www.chemcatchem.org



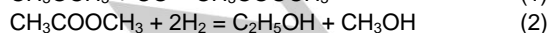
Impact of the Oxygen Vacancies on Copper Electronic State and Activity of Cu-Based Catalysts in the Hydrogenation of Methyl Acetate to Ethanol

Yushan Xi, Yue Wang*, Dawei Yao, Antai Li, Jingyu Zhang, Yujun Zhao, Jing Lv and Xinbin Ma

Abstract: Reducible oxides supported copper-based catalysts have been widely used in ester hydrogenations due to their excellent catalytic performance. However, the role of surface oxygen vacancies is still unclear. Here, we fabricated four copper-based catalysts using different shaped CeO₂ nanocrystals as supports for the hydrogenation of methyl acetate (MA) to ethanol. The catalytic activities significantly changed depending on the morphology of supports in the order of rod > cube > spindle > octahedron, which was in line with the trend of the formation energy of oxygen vacancies on the corresponding exposed lattice planes. Combined with the results of chemisorption and *in situ* FTIR experiments, it is demonstrated that the oxygen vacancies are not the primary active sites for MA hydrogenation, whereas they could significantly affect the electronic state of copper species. Under reduced conditions, the mobile oxygens could be released from the lattice and form lots of oxygen vacancies, which could strongly interact with copper particles and benefit for the generation and stabilization of Cu⁺ species. Thus, increasing the oxygen mobility of supports could effectively increase the amount of surface Cu⁺ species and enhance the catalytic activity for MA hydrogenation.

Introduction

With the reducing crude oil reserves and increasing demands for energy resources, the development of alternative routes for valuable products synthesis from syngas, which can be derived from coal, natural gas or biomass, has attracted a lot of attentions. Ethanol is a versatile feedstock and a promising fuel alternative or additive.^[1] In particular, ethanol is widely blended into the gasolines, which significantly reduced the emissions of CO, particulates and NO_x. Recently, a new route of ethanol synthesis from syngas via dimethyl ether carbonylation and methyl acetate (MA) hydrogenation has been proposed (Eq. 1-2)^[2] and shown high potential in industry. Since the hydrogenation of MA is one of the crucial steps, the design and fabrication of catalyst, and the deep understanding of the structure-function relationship are worth to be put in great efforts.



Copper species are considered as excellent catalytic active

sites in vapor-phase chemoselective hydrogenation reactions of esters to alcohols accounting for their selective hydrogenolysis of C-O bonds.^[2b] Recently, a synergistic catalysis mechanism has been proposed between Cu⁰ and Cu⁺ species in MA hydrogenation: while Cu⁰ dissociatively adsorbed H₂, Cu⁺ stabilized the methoxy and acyl species.^[3] In our previous work, the balancing effect of two active species was revealed. When the accessible metallic Cu surface area was below a certain value, the catalytic activity of hydrogenation linearly increased with the increasing Cu⁰ surface area, whereas it was primarily affected by the amount of Cu⁺ surface area.^[3b] Thus, besides enhancing copper dispersion, how to improve the amount of Cu⁺ surface area requires great efforts to study. Cu-based catalysts supported on the CeO₂,^[4] TiO₂^[5] and ZrO₂^[6] or modified by LaO_x,^[7] MnO_x^[8] and ZnO^[3a,9] additions have been reported to perform excellent activity. Notably, all of these supports or additions are reducible oxides, which may generate oxygen vacancies in the reduction condition.^[10] Li and co-workers proposed that surface oxygen vacancies of CuMnAlO_x mainly contributed to the carbonyl group adsorption of esters.^[8] However, it remains controversial about the precise role of the reducible oxides, especially about the role of the surface oxygen vacancies in MA hydrogenation.

CeO₂, as a typical defective oxide, has been widely used in catalysis, owing to its unique oxygen storage capability (OSC) and excellent redox property resulting from the rich oxygen vacancies.^[11] In hydrogenation reactions, the abundant H₂ can easily induce the generation of oxygen vacancies,^[12] which may have a great impact on the active species distribution and the catalytic activity. With recent advances in nanomaterial synthesis, it has been discovered that the oxygen vacancies are highly influenced by the morphology of ceria.^[13] Thus, applying shape-controlled CeO₂ nanocrystals as supports is a possible way to manipulate the oxygen vacancy concentration in metal/CeO₂ catalysts for a deep understanding of the relationship between the oxygen vacancy concentration and the catalytic behavior.

Herein, we synthesized CeO₂ rods, cubes, octahedrons and spindle-like nanocrystals which were reported to dominantly expose {110}, {100} or {111} facets respectively,^[14] and applied them as the supports to prepare Cu/CeO₂ catalysts. The reduced catalysts presented significant support-morphology-dependent activities in MA hydrogenation. After detailed study of the copper electronic state and the MA adsorption process, we demonstrated the role of oxygen vacancies in MA hydrogenation, which may bring new thoughts in further design of catalysts.

Results and Discussion

[a] Yushan Xi, Dr. Yue Wang*, Dawei Yao, Antai Li, Jingyu Zhang, Dr. Yujun Zhao, Dr. Jing Lv and Pro. Xinbin Ma
Key Laboratory for Green Chemical Technology of Ministry of Education, Collaborative Innovation Centre of Chemical Science and Engineering, School of Chemical Engineering and Technology, Tianjin University, Tianjin 300072, China
E-mail: yuewang@tju.edu.cn

Textual properties and catalytic performance

To investigate the role of supports with different facets exposed, the morphologies of reduced Cu/CeO₂ catalysts should be first defined. Transmission electron microscopy (TEM) images are shown in Figure 1. It is noticeable that the CeO₂ rods, cubes, octahedrons and spindle-like nanocrystals were successfully synthesized and their shapes and crystal planes were perfectly maintained during the following procedures of catalyst preparation. We can clearly see the staggered distributed nanorods with a growth direction along [110] from Figure 1a. The light points on the crystalline surfaces indicate the existence of many lattice defects. The TEM images in Fig 1c and 1e display that the obtained nanocubes and octahedrons possess pretty perfect morphology with smooth surfaces and little lattice defects, implying the good crystallinity of them. From their corresponding fast Fourier transform (FFT) patterns (insets of Figure 1d and 1f), the predominately exposed planes of cubes and octahedrons can be defined as (100) and (111), respectively. As shown in Figure 1g, the spindle-like CeO₂ nanocrystals have been obtained. The ends of them are sharp and the edges are curving, meaning that a large amount of defected sites exists. The FFT analysis suggests that the spindle-like crystals display clear (111) planes.^[14] X-ray diffraction (XRD) patterns of the CeO₂ nanoparticles (Figure S1) were collected as well. In Figure S1, all the peaks of CeO₂ nanoparticles can be ascribed to a *Fm*3*m* cubic fluorite structure (JCPD04-0593), and the peaks of Ce(OH)₃ are absent indicating the good purity of the as-prepared CeO₂. Compared with the cube and octahedron, the peaks of rod and spindle are weak and wide, which shows the poor crystallinity, i.e. lots of lattice defects existing,^[14] which is consisted with the TEM images. Thus, the specific lattice planes are exposed by different nanocrystals as we designed.

The copper species were loaded on CeO₂ crystals by ammonia evaporation method. The copper contents were determined by inductively coupled plasma optical emission spectrometer (ICP-OES). It is shown all catalysts have a similar copper loading, which is close to the designed value of 10 wt.% (Table S1). From TEM images (Figure 1) and XRD patterns of the reduced 10Cu/CeO₂ samples (Figure 2), it is demonstrated that through ammonia evaporation method and the following reduction process, the structures of CeO₂ nanoparticles were well remained. As shown in the white circle of Figure 1, the metallic Cu nanoparticles supported on CeO₂ can be seen clearly after reduction. The contrast fluctuations shown in the bulk of Cu particles are moiré fringes that arise owing to partial overlapping with other particles.^[15] No obvious sintering of copper can be seen in the TEM images. The average sizes of copper particles were counted and listed in Table 1. In Figure 2, the diffraction peaks at 2θ angles of 43.3° and 50.4° are attributed to metallic Cu (JCPDS 04-0836). The sizes of Cu nanoparticles can be calculated using the Scherrer formula (listed in Table 1). The sizes calculated by XRD are slightly larger than those counted from the TEM images, which is possibly caused by the presence of some small copper particles such as the white circled ones in Figure 1.^[16] The results suggest that the sizes of Cu⁰ in the four samples are basically identical (about 20 nm), which is confirmed by the similarity of the peak

positions in H₂ temperature programmed reduction (H₂-TPR) profiles of catalysts (Figure S2) as well. In addition, the extremely weak peak at 36.4° ascribed to Cu₂O (JCPDS 65-0328) is only observed in 10Cu/CeO₂-Spindle, and no obvious diffraction peaks of other crystal faces of Cu₂O can be observed, which implies that the Cu⁺ species are probably highly dispersed in the reduced Cu/CeO₂ catalysts.^[17]

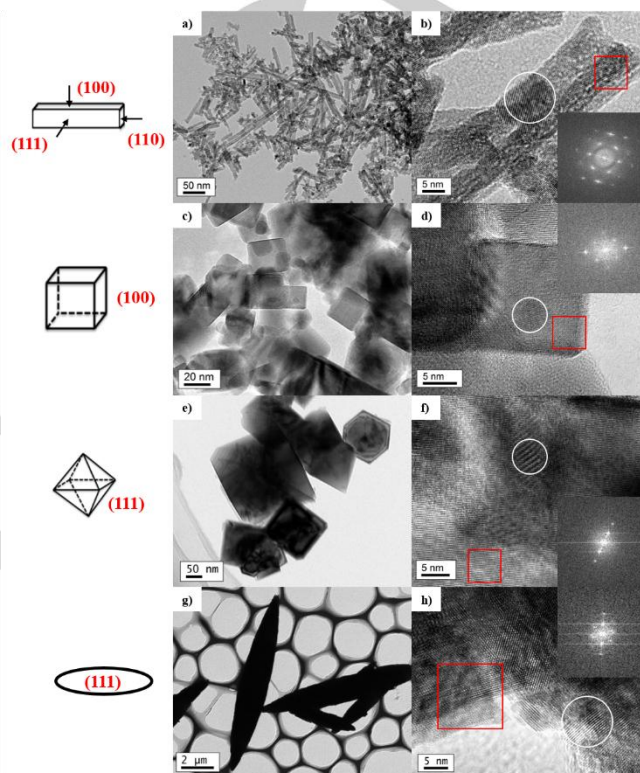


Figure 1. TEM images and their FFT of the selected area in the red box and the corresponding structural models (insets of the left ones) of the reduced 10Cu/CeO₂ catalysts with different morphologies: a) and b) Rod; c) and d) Cube; e) and f) Octahedron; g) and h) Spindle. The Cu nanoparticles are shown in the white circle.

The catalytic performance tests of the reduced Cu/CeO₂ catalysts were carried out at 488 K, 2.5 MPa with the H₂/MA of 80 in feed. As shown in Table 1, even with the similar particle size of metallic copper, the catalytic activities for MA hydrogenation varied significantly depending on the morphology of the supports, which decreased in order of rods > cubes > spindle-like > octahedrons nanocrystal as supports. By-products include methanol, ethyl acetate (EA), acetaldehyde, dimethyl ether, etc. Remarkably, 10Cu/CeO₂-Rod catalyst exhibits the best catalytic performance. The MA conversion of the catalysts supported on CeO₂ nanorods is over 5 times higher than that of supported on octahedrons. What the substantial structure is to induce these differences among catalytic performances needs to be further investigated. Consistent with other reports,^[3b,18] the selectivity of ethanol changes parallel to the MA conversion. As the MA conversion increased, the selectivity of ethanol

increased and the selectivity of EA decreased. It is because the faster hydrogenation of EA to ethanol greatly enhanced the ethanol selectivity at higher MA conversions.^[18b,19]

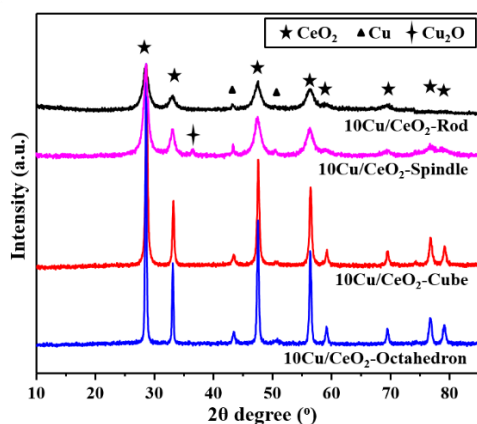


Figure 2. XRD patterns of the reduced 10Cu/CeO₂ catalysts with different morphologies.

To study the contribution of oxygen defects to the reaction, the texture factors such as pore structure should be first excluded. N₂ adsorption-desorption isotherms were measured to calculate the specific surface areas and the pore structures of the catalysts. As shown in Figure S3, there is a hysteresis loop in the isotherms of all samples demonstrating the mesoporous structure in all materials. For spindle-like sample, the pores mainly centered at about 4 nm but there are also some micropores, which consisted with the reported literature.^[14] Moreover, the pore sizes of all samples distributed in a relatively wide range. Combined with the few defects observed in nanocrystals, it could be deduced most pores are generated by the accumulation of nanocrystals, which would not hinder the reactants diffusion.^[20] It is also worthy noticed that the specific surface areas (Table S1) of rods and spindles are around 100 m²/g and those of cubes and octahedrons are much smaller. The four catalysts possess parallel mesoporous structures, but the specific surface areas of some of them exit great distances. However, even with the similar BET surface areas, the catalytic activity of 10Cu/CeO₂-Rod is still over 3 times higher than that of spindles. Thus, to study the critical factors on catalytic performance, the active sites distribution, contribution and their formation process should be primarily discussed.

Table 1. Copper contents, particle sizes of Cu/CeO₂ catalysts and the catalytic performances for MA hydrogenation.

10Cu/CeO ₂	Cu contents ^[a] (wt.%)	Crystallite size (nm)		MA conversion ^[c] (%)	Selectivity (%)		
		XRD ^[b]	TEM		Ethanol	EA	Others ^[d]
Rod	9.5	18.3	17.1	93.0	91.4	8.4	0.2
Cube	9.8	19.3	16.7	35.5	61.4	38.5	0.1
Octahedron	9.7	17.7	16.4	17.3	57.6	42.3	0.1
Spindle	9.8	22.8	19.8	25.8	59.2	40.6	0.1

[a] Metal loading was determined by ICP-OES. [b] Diameter of Cu particles calculated from XRD data by Scherrer equation. [c] Reaction conditions: catalyst weight = 0.5 g, P = 2.5 MPa, T = 488 K, H₂/MA = 80, and WLHSV_(MA) = 0.5 h⁻¹. [d] Others: CH₃CHO, C₂H₆O, etc.

Characterization of surface copper species and oxygen vacancies

Although the particle sizes of metallic copper are similar among all catalysts, the Cu⁺ species would form using CeO₂ as supports. And the amount of surface oxygen vacancies would be influenced by the morphology of nanocrystals^[13a], as well as may be boosted during reduction with the presence of copper.^[10] Thus, it is necessary to quantitatively measure the surface areas of copper species and oxygen vacancies in the reduced Cu/CeO₂ catalysts.

In literatures, N₂O titration is used as a typical method for characterization of metallic copper dispersion and surface areas.^[3b] However, for the reducible supports, the oxygen vacancies would participate in the N₂O oxidation and H₂

reduction process, leading to an inaccurate result. Here, we used a combined method of H₂-TPR, N₂O-CO titration, X-ray photoelectron spectra (XPS) and Auger electron spectroscopy (AES) to determine the amounts of surface sites (Figure S6),^[8,21] which detailed procedures are described in the Experimental Section and the results are shown in Table 2. Two peaks at 932.0 eV and 951.8 eV are shown in Cu 2p XPS (Figure 3a), which are typically assigned to the binding energy of Cu 2p_{3/2} and Cu 2p_{1/2} respectively. There are no satellite peaks at 942-944 eV, demonstrating the absence of Cu²⁺ species after reduction.^[22] In this case, we can use the asymmetrical and broad peaks in the Cu LMM AES (Figure 3b) to distinguish Cu⁰ and Cu⁺ species, which peaks centred at binding energy of 568.7 eV and 572.1 eV respectively. Thus, the specific surface areas of Cu⁰ and Cu⁺ sites can be calculated combined with the

results obtained from N₂O-CO titration (listed in Table 2).^[22] The amounts of surface Cu⁰ species are similar among the catalysts, consisted with the XRD and TEM results, while the amounts of

surface Cu⁺ species change a lot. It is demonstrated that the surface area of Cu⁺ supported on the nanorods is much larger than that supported on other ceria nanocrystals.

Table 2. Surface areas of copper species and oxygen vacancies in the reduced Cu/CeO₂ catalysts.

10Cu/CeO ₂	S _{Cu⁰} ^[a] (m ² /g)	X _{Cu(I)} ^[b] (%)	S _{Cu⁰} ^[c] (m ² /g)	S _{Cu(I)} ^[c] (m ² /g)	S _{O_v} ^[d] (m ² /g)	A _{Cu(I)} ^[e] (area)
Rod	46.0	87.6	5.7	40.3	73	22.6
Cube	19.9	73.9	5.2	14.7	10	8.7
Octahedron	9.4	38.3	5.8	3.6	52	2.8
Spindle	9.3	47.3	4.9	4.4	37	3.2

[a] Assuming that the Cu⁺ and Cu⁰ species occupy identical areas, the total surface area of Cu species is calculated from the CO uptake in N₂O-CO titration. [b] Cu⁺/(Cu⁺ + Cu⁰) was calculated from the Cu LMM AES. [c] The surface area of Cu⁰ and Cu⁺ species are calculated combining the N₂O-CO titration and AES results. [d] The surface area of oxygen vacancies is determined combining the N₂O-CO titration and N₂O-TPR. [e] Integral area under the peaks of Cu⁺-CO species in the FTIR spectra of CO adsorption after evacuation.

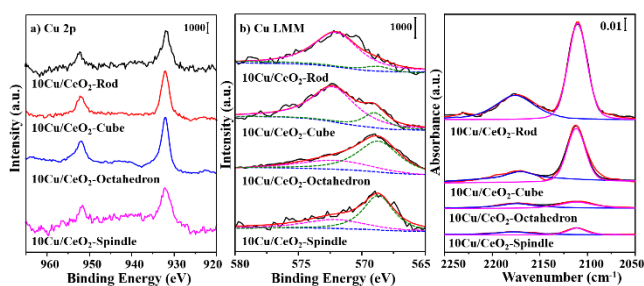


Figure 3. a) Cu 2p XPS spectra, b) Cu LMM AES spectra and c) *in situ* FTIR of CO adsorption spectra of the reduced 10Cu/CeO₂ catalysts with different morphologies.

In situ Fourier transform infrared (FTIR) of CO absorption are used to verify the obtained results of surface sites. For the Cu⁰-CO and Cu²⁺-CO bonds are very weak as reported and no Cu²⁺ species existed after reduction, the obtained peaks in Figure 3c could be attributed to CO adsorbed on Cu⁺ species.^[23] The band at 2110 cm⁻¹ could be assigned to CO adsorbed on associated Cu⁺ species while the broad band around 2177 cm⁻¹ is attributed to isolated ones.^[3b] The experiments were carried out using CeO₂ nanocrystals as blank samples as well (Figure S4). There is no obvious peak at 2050-2250 cm⁻¹. After calculation, it is demonstrated that the integrated areas of the Cu⁺-CO peaks (A_{Cu(I)}) is linearly changed with S_{Cu(I)} (Figure S5), which verified the correction of characterization results of surface Cu species.

The role of oxygen vacancies in MA hydrogenation

A lot of papers have demonstrated that the cooperation of Cu⁰ and Cu⁺ active species is the key to achieve excellent

catalytic performance in ester hydrogenations, where Cu⁰ facilitated the H₂ decomposition while Cu⁺ sites adsorbed the methoxy and acyl species.^[3b,22] Recently, Li and co-workers^[8] proposed that the synergy between active Cu⁰ species and surface Mn²⁺-O_v-Mn²⁺ defect structures, rather than Cu⁺ species, was responsible for the high catalytic efficiency of CuMnAlO_x for dimethyl succinate hydrogenation. It was demonstrated that the surface vacancies could strongly interact with the carbonyl group, thus weakening the C=O and promoting the hydrogenation. But in the work of Ru/CeO₂ for CO₂ methanation, there is no positive correlation between the methanation activity and the concentration of oxygen vacancies.^[24] Thus, whether the oxygen vacancies act as active sites needs further investigation.

Catalytic performance was correlated with the surface areas of Cu⁰, Cu⁺ species and oxygen vacancies respectively (shown in Figure 4) to reveal the role of oxygen vacancies in MA hydrogenation. The surface areas of Cu⁰ species among the four catalysts are similar, which are negligible for discussion. It is displayed that the catalytic activity is linearly increased with the increasing amount of surface Cu⁺ species, indicating that the surface Cu⁺ species should play a key role in enhancing the catalytic activity for MA hydrogenation, whereas the scatters in the correlation plot between activity and S_{O_v} suggests that the surface oxygen vacancies are not the main factor of affecting the catalytic performance.

To further illustrate the contributions of surface Cu⁺ and oxygen vacancies in MA hydrogenation, *in situ* FTIR of MA adsorption was performed with 10Cu/CeO₂-Rod and the corresponding support respectively. Figure 5a and 5b are the FTIR spectra of the two samples collected during the process of MA adsorption. The bands at 1778 and 1760 cm⁻¹ are assigned to the C=O stretching in gaseous MA, and the bands at 1255 and 1247 cm⁻¹ are ascribed to the hydroxyl bending of MA in gas phase.^[25] These four intense bands appeared immediately after the samples were exposed to MA, and the intensity decreased

with time due to the adsorption and dissociation of MA. It can be seen that the intensities of bands at ~ 1440 , 1374 and 1600 cm^{-1} , which are related to the C-H bending, O-C-O stretching and C=O stretching modes of adsorbed MA or acetyl species respectively, were increased gradually according to the trend over time. These changing trends happened in both $10\text{Cu}/\text{CeO}_2$ -Rod and CeO_2 -Rod samples, indicating that MA can be adsorbed on both catalyst and support, and some of them may be dissociated to methoxy and acyl species. The results suggest the surface oxygen vacancies could indeed enhance the adsorption and dissociation of MA. However, the difference of abilities to adsorb and activate MA between the two samples appeared after evacuation. Compared to $10\text{Cu}/\text{CeO}_2$ -Rod, the spectrum of CeO_2 -Rod after evacuation displayed two very weak and broad bands at 1633 and 1400 cm^{-1} , which are assigned to the asymmetric and symmetric stretching vibrations of acetyl group respectively.^[26] Thus, based on the above investigation, it can be concluded that although the surface oxygen vacancies are conducive to MA adsorption and dissociation, compared to Cu^+ species, its ability is too weak to be the key factor for influencing the catalytic performance. In addition, the TOF value of Cu^0 species shows a linear positive correlation with $S_{\text{Cu}(0)}$. (Figure S7) It is indicated that the surface Cu^+ is the main factor affecting catalytic performance when the influence of surface

Cu^0 is normalized, which is consistent with the above analysis. Considering the big difference of Cu^+ species among the four catalysts, the role of oxygen vacancies may reflect in affecting the copper electronic state distribution.

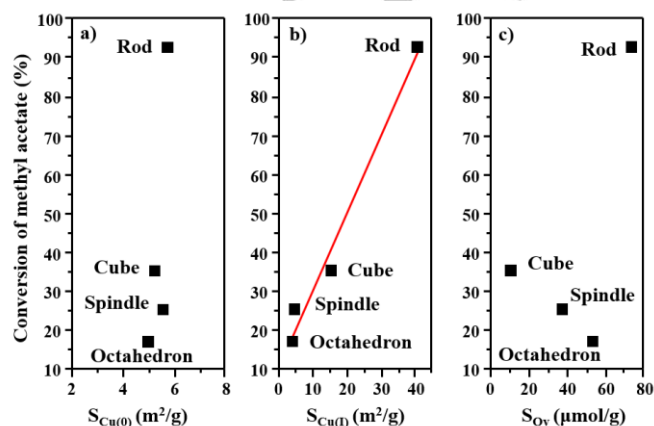


Figure 4. Correlation of MA conversion with the amounts of a) Cu^0 sites, b) Cu^+ sites and c) oxygen vacancies on the surface of reduced Cu/CeO_2 catalysts.

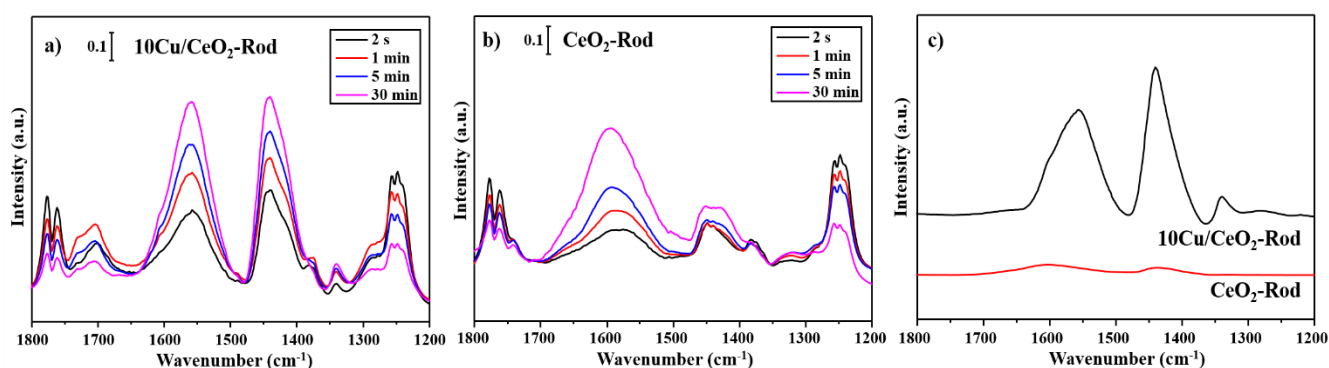


Figure 5. *In situ* FTIR spectra of MA adsorption of the reduced $10\text{Cu}/\text{CeO}_2$ -Rod and CeO_2 nanorods: a) and b) the spectra during MA adsorption process; c) the final spectra after evacuation, which was collected when the spectrum no longer changed.

We propose the role of oxygen vacancies of CeO_2 support is mainly interacting with Cu particles and benefiting for Cu^+ species generation and stabilization. In the reductive conditions, the mobile oxygens can be released from the lattice and form lots of oxygen vacancies. The oxygen mobility (OM) of the CeO_2 nanocrystals was measured to follow the order of rods > cubes > spindle-like > octahedrons (Table S2). Given the certain facets they exposed, the results are consistent with the reports that the calculated oxygen vacancy formation energies are displayed in order of $(110) < (100) < (111)$.^[13a,27] It is observed by TEM that the spindle-like nanocrystals have much more lattice defects than the octahedrons, which can explain the OM difference between them. The significant effect of oxygen mobility of

supports on the distribution of Cu species is demonstrated in Figure 6. The amounts of Cu^+ sites are linearly increased with the increasing OM of CeO_2 nanocrystals, which strongly supported our opinion. Thus, the catalytic performance for MA hydrogenation is significantly enhanced by the increasing amount of surface Cu^+ sites, which are generated and stabilized by the strong interaction between Cu species and the oxygen vacancies of supports.^[28] Concerning the oxygen vacancies, their formation energies are dominantly affected by the exposed facets, which are dependent on the morphology of CeO_2 nanocrystals. The CeO_2 nanorods, which exposed crystal planes of $\{110\}$ with the lowest oxygen vacancy formation energy, presented the highest activity in MA hydrogenation.

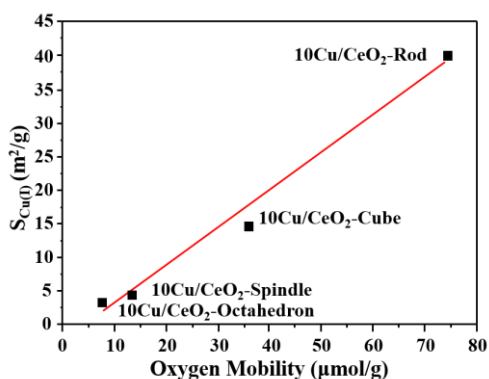


Figure 6. The effect of oxygen mobility of CeO₂ nanocrystals on the surface Cu⁺ species area of reduced catalysts.

Conclusions

In summary, the Cu-based catalysts supported on shape-controlled CeO₂ nanocrystals were fabricated and exhibited significantly support-morphology dependent catalytic activity in MA hydrogenation. The catalytic performance increases linearly with the increasing amount of surface Cu⁺ sites, and the amounts of Cu⁺ species are found to be dominantly affected by the mobile oxygen vacancy concentration of CeO₂ supports, which is associated with the crystal facets exposed. Moreover, the contribution of surface oxygen vacancies in reaction was investigated as well. Although the surface oxygen vacancies could adsorb and dissociate MA, compared to Cu⁺ species, its ability is too weak to be the key active species in the hydrogenation reaction. The significant role of oxygen vacancies is reflected in the strong interaction with copper particles, which benefits for the Cu⁺ generation and stabilization. These results may provide new possibilities for the rational design of catalyst according to a deep understanding of the contribution of supports to the active sites distribution and the catalytic activity in hydrogenation reactions.

Experimental Section

Chemicals

Ce(NO₃)₂·6H₂O (99.99%, AR), Cu(NO₃)₂·3H₂O (≥ 99%), aqueous ammonia solution (25-28 wt.%) and carbamide (≥ 99.3%, AR) were purchased from Sinopharm Chemical Reagent Co., Ltd (Beijing, China). NaOH (≥ 96.0%, AR) and Na₃PO₄·12H₂O (≥ 99.6%, AR) were obtained from Tianjin Guangfu Fine Chemical Research Institute (Tianjin, China). All chemicals were used without any treatment or purification.

Catalyst preparation

All of the CeO₂ nanocrystal supports were prepared using the hydrothermal method.^[14] The procedures of preparing CeO₂ nanorods and nanocubes are listed as follows. 4 mmol Ce(NO₃)₃·6H₂O and 480 mmol NaOH were dissolved in deionized water respectively then mixed together and stirred for 30 min. The suspension was transferred into

autoclave and heated for 24 h at 373 K (453 K) to get nanorods (nanocubes). After filtered, washed and dried, the precipitates were calcined at 673 K for 4 h. For the synthesis of CeO₂ nanooctahedrons and nanospindles, the procedures were basically the same as described above except the chemicals and hydrothermal treatment conditions. For nanooctahedrons, 2 mmol Ce(NO₃)₃·6H₂O and 0.02 mmol Na₃PO₄·12H₂O were used and the following hydrothermal treatment was at 433 K for 12 h. 2.4 mmol Ce(NO₃)₃·6H₂O and 6.4 mmol carbamide were used to fabricate nanospindles and the autoclave was heated at 393 K for 8 h.

The Cu/CeO₂ catalysts were synthesized by the ammonia evaporation method. First, 2.5 g CeO₂ nanocrystals was added to 100 mL of deionized water and 23 mL aqueous ammonia solution and stirred at 303 K for 1 h. After heated to 353 K, a solution of 1.056 g Cu(NO₃)₂·3H₂O was added to the suspension and then started the ammonia evaporation. This process was terminated when the pH value decreased to 6-7. The precipitate was filtered, washed, dried and calcined at 673 K for 4 h, and then tableted, crushed and sieved to 40-60 meshes.

Catalyst characterization

N₂ adsorption-desorption analysis was measured by Micromeritics Tristar 3000. The specific surface area and pore size distribution was calculated by Brunauer-Emmett-Teller (BET) method and Barrett-Joyner-Halenda (BJH) method respectively. Transmission electron microscopy (TEM) images were obtained by Philips TECNAI G2 F20 system electron microscope with field emission gun. Inductively coupled plasma optical emission spectrometer (ICP-OES, Varian Vista-MPX) was applied to test Cu content of catalysts. Powder X-ray diffraction (XRD) were conducted on Rigaku C/max-2500 diffractometer with a graphite-filtered Cu K α radiation ($\lambda = 1.5406 \text{ \AA}$).

X-ray photoelectron spectra (XPS) and Auger electron spectroscopy (AES) were carried out on PHI 1600 ESCA (PE Company) with an Al K α X-ray radiation source ($h\nu = 1486.6 \text{ eV}$). We pressed catalysts to thin disks and reduced them in a flow of H₂ at 523 K for 4 h. After cooling to room temperature, the samples were transferred to a holder immediately in a glove-box filled with N₂ and then outgassed in chamber, which guaranteed the states of surface Cu species in the reduced catalysts were measured correctly. The binding energies were calibrated using the C 1s peak at 284.6 eV as the reference. The experimental errors were within $\pm 0.2 \text{ eV}$.

Combining H₂-TPR, N₂O oxidation and CO pulse chemisorption, the surface areas of copper species and oxygen vacancies in the reduced Cu/CeO₂ catalysts were obtained using a Micromeritics Autochem II 2920 apparatus.^[8,21] The sample was reduced with 10% H₂/Ar at 523 K, when the Cu²⁺ turned to Cu⁰ or Cu⁺ species and oxygen vacancies generated in CeO₂. After cooling down to 363 K in Ar flow, the sample was exposed in N₂O for 1 h to oxidize surface Cu⁰ to Cu⁺ species, as well as the surface oxygen vacancies. Following, a typical CO chemisorption was conducted at 323 K, which results reflected the total amount of surface copper species. Thus, the surface areas of copper species ($S_{Cu(0)}$ or $S_{Cu(I)}$, m²/g) can be easily calculated depending on the Cu⁺/(Cu⁰+Cu⁺) ratios ($X_{Cu(I)}$, %) from Cu LMM AES. Based on the above results, the amounts of surface oxygen vacancies in the reduced catalysts can be determined by combining the N₂O oxidation and H₂-TPR results.^[8] Instead of the typical CO chemisorption after the N₂O oxidation in the above procedure, a H₂-TPR was carried out to reduce the surface Cu⁺ species and the mobile oxygen atoms with a temperature ramp from 323 K to 523 K and held for 1 h. In this way, the amount of surface oxygen vacancies in the reduced catalysts could be calculated by subtracting the total amount of

surface copper species obtained previously from the H₂-TPR consumption.

The concentrations of oxygen vacancies in CeO₂ nanocrystals were measured by oxygen pulse injection method using a Micromeritics Autochem II 2920 as well. After reduced in 523 K for 1 h, the sample was treated under flowing He to remove the physisorbed molecular. Then the injection pulses of 10%O₂/He were carried out until the consumption peaks became stable. To simulate the cyclical oxygen activity, the above process was repeated. The oxygen reuptake was used to characterize the oxygen mobility in CeO₂, which is more representative of the pool of available surface sites for oxygen transfer during actual operation of catalysts.^[29]

In situ FTIR of CO adsorption was conducted to measure the amount of surface Cu⁺ species using a Nicolet 6700 spectrometer with *in situ* cell and vacuum system. The sample disc was settled into the cell and reduced in the flow of 10% H₂/Ar at 523 K for 1 h. After cooled to 303 K in He flow, the sample was exposed to CO at 303 K for 30 min. After that, the sample was vacuumed and spectra were collected. The last spectrum was confirmed to be no differences with the precious one.

In situ FTIR of MA adsorption was performed to identify whether surface oxygen vacancies act as active sites in MA hydrogenation. After reduction, the samples are exposed to MA at 303 K for 30 min. The spectra of MA adsorption were collected from the beginning. After that, the desorption of MA was carried out in He flow at 303 K until the spectrum was not changed.

Catalytic activity evaluation

The reactivity evaluations were carried out on a fix-bed reactor. Samples of 0.5 g calcined catalysts (40-60 meshes) were first reduced in H₂ flow at 523 K for 4 h. After cooling down to 488 K, the reaction was carried out at 2.5 MPa with a feed flow of H₂ and MA (the molar ratio of H₂ to MA is 80). The products were condensed and analysed using Agilent Micro GC 6820 with an HP-INNOWAX capillary column (30 m × 0.32mm × 0.50 μm) equipped with a flame ionization detector (FID).

Acknowledgements

We gratefully acknowledge supports from the National Natural Science Foundation of China (21706184), the Natural Science Foundation of Tianjin City (18JCQNJC06100) and the National Postdoctoral Program for Innovative Talents of China (BX20180211).

Keywords: heterogeneous catalysis • hydrogenation • copper-based catalyst • ethanol • CeO₂ • oxygen vacancy

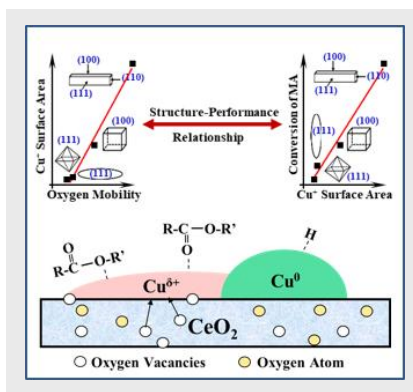
- [1] J. Goldemberg, *Science* **2007**, 315, 808-810.
- [2] a) X. San, Y. Zhang, W. Shen, N. Tsubaki, *Energ. Fuel* **2009**, 23, 2843-2844; b) X. Li, X. San, Y. Zhang, T. Ichii, M. Meng, Y. Tan, N. Tsubaki, *ChemSusChem* **2010**, 3, 1192-1199; c) G. Yang, X. San, N. Jiang, Y. Tanaka, X. Li, Q. Jin, K. Tao, F. Meng, N. Tsubaki, *Catal. Today* **2011**, 164, 425-428.
- [3] a) D.S. Brands, E.K. Poels, A. Bliiek, *Appl. Catal. A* **1999**, 184, 279-289; b) Y. Wang, Y. Shen, Y. Zhao, J. Lv, S. Wang, X. Ma, *ACS Catal.* **2015**, 5, 6200-6208; c) A. Yin, X. Guo, W.-L. Dai, K. Fan, *J. Phys. Chem. C* **2009**, 113, 11003-11013.
- [4] a) Y. Liu, K. Murata, M. Inaba, I. Takahara, *Fuel Process. Technol.* **2013**, 110, 206-213; b) H. Li, Y. Cui, Q. Liu, W.-L. Dai, *ChemCatChem* **2018**, 10, 619-624.
- [5] a) C. Wen, A. Yin, Y. Cui, X. Yang, W.-L. Dai, K. Fan, *Appl. Catal. A* **2013**, 458, 82-89; b) B. Wang, C. Wen, Y. Cui, X. Chen, Y. Dong, W.-L. Dai, *RSC Adv.* **2015**, 5, 29040-29047.
- [6] a) Y. Zhu, X. Kong, S. Zhu, F. Dong, H. Zheng, Y. Zhu, Y.-W. Li, *Appl. Catal. B* **2015**, 166-167, 551-559; b) Y. Zhu, X. Kong, D.-B. Cao, J. Cui, Y. Zhu, Y.-W. Li, *ACS Catal.* **2014**, 4, 3675-3681.
- [7] X. Zheng, H. Lin, J. Zheng, X. Duan, Y. Yuan, *ACS Catal.* **2013**, 3, 2738-2749.
- [8] Q. Hu, L. Yang, G. Fan, F. Li, *J. Catal.* **2016**, 340, 184-195.
- [9] D. Brands, E. Poels, T. Krieger, O. Makarova, C. Weber, S. Veer, A. Bliiek, *Catal. Lett.* **1996**, 36, 175-181.
- [10] Y. Wang, Z. Chen, P. Han, Y. Du, Z. Gu, X. Xu, G. Zheng, *ACS Catal.* **2018**, 8, 7113-7119.
- [11] a) G. Vilé, S. Colussi, F. Krumeich, A. Trovarelli, J. Pérez-Ramírez, *Angew. Chem. Int. Ed.* **2014**, 53, 12069-12072; b) Q. Li, Y. Zhang, G. Chen, J. Fan, H. Lan, Y. Yang, *J. Catal.* **2010**, 273, 167-176; c) Y.H. Taufiq-Yap, Sudarno, U. Rashid, Z. Zainal, *Appl. Catal. A* **2013**, 468, 359-369.
- [12] C. Sun, H. Li, L. Chen, *Energy Environ. Sci.* **2012**, 5, 8475-8505.
- [13] a) A.K.P. Mann, Z. Wu, F.C. Calaza, S.H. Overbury, *ACS Catal.* **2014**, 4, 2437-2448; b) K. Zhou, X. Wang, X. Sun, Q. Peng, Y. Li, *J. Catal.* **2005**, 229, 206-212; c) X. Liu, K. Zhou, L. Wang, B. Wang, Y. Li, *J. Am. Chem. Soc.* **2009**, 131, 3140-3141.
- [14] S. Wang, L. Zhao, W. Wang, Y. Zhao, G. Zhang, X. Ma, J. Gong, *Nanoscale* **2013**, 5, 5582-5588.
- [15] Y. Zhao, B. Shan, Y. Wang, J. Zhou, S. Wang, X. Ma, *Ind. Eng. Chem. Res.* **2018**, 57, 4526-4534.
- [16] H.C. Yao, Y.F.Y. Yao, *J. Catal.* **1984**, 86, 254-265.
- [17] M.B. Fichtl, J. Schumann, I. Kasatkin, N. Jacobsen, M. Behrens, R. Schlögl, M. Muhler, O. Hinrichsen, *Angew. Chem. Int. Ed.* **2014**, 53, 7043-7047.
- [18] a) P. Munnik, M. Wolters, A. Gabrielson, S.D. Pollington, G. Headdock, J.H. Bitter, P.E. de Jongh, K.P. de Jong, *J. Phys. Chem. C* **2011**, 115, 14698-14706; b) W.-W. Wang, P.-P. Du, S.-H. Zou, H.-Y. He, R.-X. Wang, Z. Jin, S. Shi, Y.-Y. Huang, R. Si, Q.-S. Song, C.-J. Jia, C.-H. Yan, *ACS Catal.* **2015**, 5, 2088-2099; c) Y. Wang, J. Liao, J. Zhang, S. Wang, Y. Zhao, X. Ma, *AIChE J.* **2017**, 63, 2839-2849.
- [19] X. Huang, M. Ma, S. Miao, Y. Zheng, M. Chen, W. Shen, *Applied Catal. A* **2017**, 531, 79-88.
- [20] Y. Wang, Y. Zhao, J. Lv, X. Ma, *ChemCatChem* **2017**, 9, 2085-2090.
- [21] M.A.N. Santiago, M.A. Sánchez-Castillo, R.D. Cortright, J.A. Dumesic, *J. Catal.* **2000**, 193, 16-28.
- [22] W. Zhou, Y. Zhao, Y. Wang, S. Wang, X. Ma, *ChemCatChem* **2016**, 8, 3663-3671.
- [23] L.-F. Chen, P.-J. Guo, M.-H. Qiao, S.-R. Yan, H.-X. Li, W. Shen, H.-L. Xu, K.-N. Fan, *J. Catal.* **2008**, 257, 172-180.
- [24] J. Zheng, J. Zhou, H. Lin, X. Duan, C.T. Williams, Y. Yuan, *J. Phys. Chem. C* **2015**, 119, 13758-13766.
- [25] Y. Guo, S. Mei, K. Yuan, D.-J. Wang, H.-C. Liu, C.-H. Yan, Y.-W. Zhang, *ACS Catal.* **2018**, 8, 6203-6215.
- [26] H. Zhou, W.L. Zhu, L. Shi, H.C. Liu, S.P. Liu, Y.M. Ni, Y. Liu, Y.L. He, S.L. Xu, L.N. Li, Z.M. Liu, *J. Mol. Catal. A* **2016**, 417, 1-9.
- [27] a) Y. Li, S.Y. Huang, Z.Z. Cheng, S.P. Wang, Q.F. Ge, X.B. Ma, *J. Catal.* **2018**, 365, 440-449; b) Z. Wu, M. Li, D.R. Mullins, S.H. Overbury, *ACS Catal.* **2012**, 2, 2224-2234.
- [28] M. Nolan, S.C. Parker, G.W. Watson, *Surf. Sci.* **2005**, 595, 223-232.
- [29] A. Chen, X. Yu, Y. Zhou, S. Miao, Y. Li, S. Kuld, J. Sehested, J. Liu, T. Aoki, S. Hong, M.F. Camellone, S. Fabris, J. Ning, C. Jin, C. Yang, A. Nefedov, C. Wöll, Y. Wang, W. Shen, *Nature Catal.* **2019**.

Entry for the Table of Contents (Please choose one layout)

Layout 1:

FULL PAPER

The catalytic activity changed significantly depending on the morphology of supports in order of rod > cube > spindle > octahedron, which is in line with the trend of the formation energy of oxygen vacancies on the corresponding exposed lattice planes. The oxygen vacancies are not the primary active sites for MA hydrogenation, whereas they could effectively increase the amount of surface Cu^+ species and enhance the catalytic activity for MA hydrogenation.



Yushan Xi, Yue Wang*, Dawei Yao,
Antai Li, Jingyu Zhang, Yujun Zhao, Jing
Lv and Xinbin Ma

Page No. – Page No.

**Impact of the Oxygen Vacancies on
Copper Electronic State and Activity
of Cu-Based Catalysts in the
Hydrogenation of Methyl Acetate to
Ethanol**